

# First higher-multipole model of spinning binary-black-hole gravitational waveforms

Lionel London,<sup>1</sup> Sebastian Khan,<sup>2,3</sup> Edward Fauchon-Jones,<sup>1</sup> Xisco Jiménez Forteza,<sup>4</sup> Mark Hannam,<sup>1</sup> Sascha Husa,<sup>4</sup> Chinmay Kalaghatgi,<sup>1</sup> Frank Ohme,<sup>2,3</sup> and Francesco Pannarale<sup>1</sup>

<sup>1</sup>*School of Physics and Astronomy, Cardiff University, Queens Building, CF24 3AA, Cardiff, United Kingdom*

<sup>2</sup>*Max Planck Institute for Gravitational Physics (Albert Einstein Institute), Callinstr. 38, 30167 Hannover, Germany*

<sup>3</sup>*Leibniz Universität Hannover, Institute for Gravitational Physics, Callinstr. 38, 30167 Hannover, Germany*

<sup>4</sup>*Departament de Física Universitat de les Illes Balears and Institut d'Estudis Espacials de Catalunya, Crta. Valldemossa km 7.5, E-07122 Palma, Spain*

(Dated: August 4, 2017)

Gravitational-wave observations of binary black holes currently rely on theoretical models that predict the dominant multipole radiation during the coalescence. Here we introduce a simple method to include the subdominant multipole contributions to binary black hole gravitational waveforms, given a frequency-domain model for the dominant ( $\ell = 2, |m| = 2$ ) multipoles. The amplitude and phase of the original model are appropriately stretched and rescaled using leading-order post-Newtonian results (for the inspiral), perturbation theory (for the ringdown), and a smooth transition between the two. No additional tuning to numerical-relativity simulations is required. We apply a variant of this method to the non-precessing PhenomD model. The result, PhenomHM, constitutes the first higher-multipole model of *spinning* black-hole binaries, and currently includes  $(\ell, |m|) = (2, 2), (3, 3), (4, 4), (2, 1), (3, 2), (4, 3)$ . Comparisons with a set of numerical-relativity waveforms demonstrate that PhenomHM is more accurate than PhenomD for all binary configurations, and using PhenomHM typically leads to improved measurements of the binary's properties. Our approach can be extended to precessing systems, enabling wide-ranging studies of the impact of higher harmonics on gravitational-wave astronomy, and tests of fundamental physics.

*Introduction* – Gravitational waves (GWs) are our most direct means of observing black hole (BH) binary mergers [1–3]. Measurements from Advanced LIGO (aLIGO) observations rely on the agreement between experimental data and theoretical models of the GW signal emitted during the coalescence [3–6]. To date, these models include only the dominant multipoles ( $\ell = 2, |m| = 2$ ) of the signal. This may be sufficient when the BHs have comparable masses, or the signal is weak, but for binaries where one BH is more massive than the other (even by a ratio of only 1:3 [7–10]), modelling the subdominant multipoles could significantly improve measurement accuracy, and in some cases will be necessary to avoid large biases.

Currently, higher multipoles have been modelled analytically for the entire merger only for non-spinning binaries [11], or restricted corners of the parameter space [12]. They can be calculated for individual binary configurations from Numerical Relativity (NR) simulations (see Fig. 1), but an analytical, higher-multipole model of spinning binaries would be extremely valuable. Even an approximate model would make it possible to assess the importance of higher multipoles in interpreting a GW observation.

This need has motivated the flexible construction we present here: starting from an accurate model for the dominant multipoles, we use a set of basic results from Post-Newtonian (PN) and perturbation theory to map the dominant multipole into each of the other multipoles. Our approach can be applied to any frequency-domain model, and we expect that it will accelerate the further development of higher-multipole models. Here we construct an explicit model by extending PhenomD [13], and we demonstrate the accuracy improvement when higher multipoles are added, particularly for source distance and orientation.

Figure 2 illustrates the impact of higher multipoles. We calculate the total GW strain,  $h = h_+ - i h_\times$ , for the system shown in Fig. 1 with a total mass of  $50M_\odot$ , at a distance of 500 Mpc, and at varying inclination angles. We see that as the inclination changes from face-on ( $\iota = 0$ ) toward edge-on ( $\iota =$

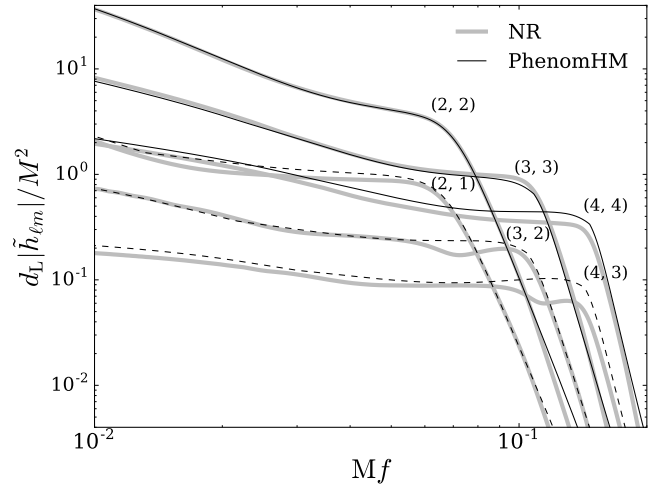


Figure 1. A GW signal decomposed into its multipolar contributions, for a nonspinning binary with a mass ratio of 1:8. Our new model (PhenomHM) is included as thin black lines. Solid lines are  $m = \ell$  multipoles and dashed lines are  $m = \ell - 1$ . NR multipoles are displayed in gray, thick lines.

$\pi/2$ ), the signal develops more structure, and becomes weaker. We also see that our new model reproduces the signal far more accurately than the dominant-multipole model. It is important to emphasize that this level of agreement is achieved without any tuning to NR waveforms.

*Methods* – We consider the GW strain decomposed into spherical harmonics with spin weight  $-2$  [16],

$$h(t, \vec{\lambda}, \theta, \phi) = \sum_{\ell \geq 2} \sum_{-\ell \leq m \leq \ell} h_{\ell m}(t, \vec{\lambda}) {}^{-2}Y_{\ell m}(\theta, \phi), \quad (1)$$

where  $t$  is the time,  $\vec{\lambda}$  denotes the intrinsic parameters (masses, spins),  $\theta$  and  $\phi$  are the spherical angles in a source-centered coordinate system in which the  $z$ -axis points along the orbital angular momentum. We now describe transformations

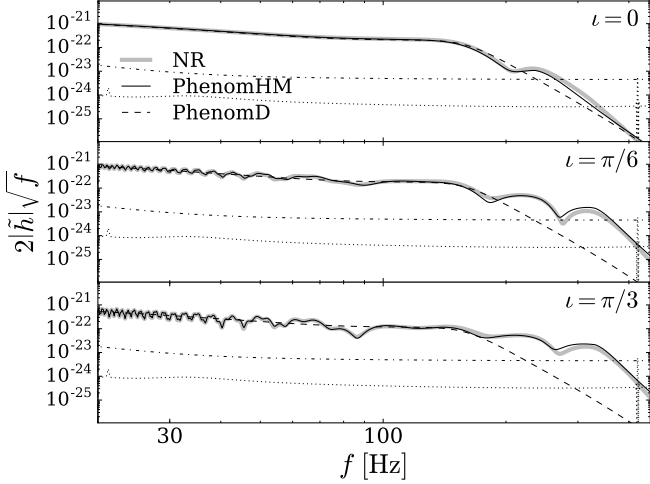


Figure 2. The GW signal amplitude of a nonspinning BH binary with mass ratio 1:8, total mass  $90M_\odot$ , at a distance of 500 Mpc, optimised over initial orbital phase  $\phi_0$ , and inclination angle  $\iota$  equal to 0,  $\pi/6$ ,  $\pi/3$ , from top to bottom. In each panel, the NR data are displayed in gray, thick lines. The PhenomHM and PhenomD models are shown in thick black lines which are continuous and dashed, respectively. Modelled aLIGO and Einstein Telescope noise spectral densities [14, 15] are displayed in dashed-dotted and dotted black lines.

between the Fourier representations  $\tilde{h}_{22}$  and the various subdominant multipoles  $\tilde{h}_{\ell m}$  by using the analytic relationships of PN and BH perturbation theory. At this stage we make no further assumptions about the model; our approach can be applied to any non-precessing waveform model. Noting that additional refinements can be made once a model for the dominant multipole is chosen, we then present a variation of our method applied to PhenomD.

If we look at the example in Fig. 1, we see that all of the multipole amplitudes are qualitatively similar; an appropriate scaling and stretching of the dominant (2,2) amplitude could conceivably be sufficient to approximately reproduce each of the other multipoles. A similar observation applies to the phase of the signal (or the phase derivative, which is often a more instructive quantity [17]). We construct a simple transformation that achieves this.

We separate each GW multipole into amplitude  $A_{\ell m}(f)$  and phase  $\varphi_{\ell m}(f)$ ,

$$\begin{aligned} \tilde{h}_{\ell m}(f) &= A_{\ell m}(f) \times \exp[i\varphi_{\ell m}(f)] \\ &\approx \beta_{\ell m}(f_{\ell m}^A) A_{22}(f_{\ell m}^A) \times \exp\left\{i\left[\kappa_{\ell m}\varphi_{22}(f_{\ell m}^\varphi) + \Delta_{\ell m}\right]\right\}. \end{aligned} \quad (2)$$

Equation (3) is written to emphasize that we construct  $\tilde{h}_{\ell m}$  by mapping the leading multipole radiation into the higher multipoles in a manner that will operate separately on the frequency domain values,  $f_{\ell m}(f)$ , and the related amplitude and phase functions,  $A_{22}$  and  $\varphi_{22}$ . As we will show below, the frequency, amplitude and phase mappings are simple scaling relations. For compactness, we therefore refer to our procedure as *dominant-multipole scaling*.

Our construction is motivated by three aspects of PN and Quasi-Normal Mode (QNM) theory. First, we note that during inspiral, the oscillation frequency of each  $(\ell, m)$  multipole (in the time-domain) is approximately  $m\Omega$ , where  $\Omega$  is the orbital frequency of the binary. Therefore, the frequency  $f$  of each

multipole corresponds to a  $(2, 2)$ -mode frequency of  $2f/m$ . This relationship is exact in the low-frequency limit of closed circular orbits, from the symmetry of the system.

Second, the stationary phase approximation (SPA) allows the association of these frequencies with values in the  $\tilde{h}_{\ell m}(f)$  domain [18]. Simultaneously, the SPA predicts to leading-order in  $f$  the amplitude scaling of each multipole (relative to the  $\ell = |m| = 2$  multipole),  $\beta_{\ell m}(f)$ , which approximately relates the amplitudes of different  $\tilde{h}_{\ell m}$ 's.

$$\begin{aligned} \beta_{22} &= 1, & \beta_{21} &= \left(\frac{1}{2}\right)^{-5/6} \frac{\delta}{3} F^{1/3}, \\ \beta_{33} &= \left(\frac{3}{2}\right)^{-5/6} \sqrt{\frac{135}{224}} \delta F^{1/3}, & \beta_{32} &= \sqrt{\frac{5}{63}} (\delta^2 + \eta) F^{2/3}, \\ \beta_{44} &= \sqrt{\frac{160}{567}} (\delta^2 + \eta) F^{2/3}, & \beta_{43} &= \left(\frac{3}{2}\right)^{-1/6} \sqrt{\frac{81}{1120}} (\delta^2 + 2\eta) \delta F \end{aligned} \quad (4)$$

and where we define  $\delta = |m_1 - m_2|/M$ ,  $M = m_1 + m_2$ ,  $\eta = m_1 m_2 / M^2$ ,  $F = \pi M f$ . Here, an additional scaling factor ( $m/2$  to the leading order frequency power of each multipole) has been added to recover correct overall scaling in Equation (3).

Lastly, we note that in the vicinity of the multipole's fundamental ringdown frequency, QNM theory implies that the frequencies of different  $\tilde{h}_{\ell m}$  are related by a simple linear shift.

To bridge the ‘‘gap’’ between the PN and QNM regimes, we find that linear interpolation is sufficient. The result of this choice is a piecewise-linear mapping,

$$f_{\ell m}(f) = \begin{cases} \frac{2}{m}f, & f \leq f_0 \\ \frac{f_{22}^{\text{RD}} - 2f_0/m}{f_{\ell m}^{\text{RD}} - f_0} (f - f_0) + \frac{2f_0}{m}, & f_0 < f \leq f_{\ell m}^{\text{RD}} \\ f - f_{\ell m}^{\text{RD}} + f_{22}^{\text{RD}}, & f > f_{\ell m}^{\text{RD}}. \end{cases} \quad (5)$$

We optimized the agreement with NR simulations by allowing different values of  $f_0$  for the amplitude and phase, hence the distinction between  $f_{\ell m}^A$  and  $f_{\ell m}^\varphi$  in Equation (3). Here we use  $f_0^A = 0.018 f_{\ell m}^{\text{RD}} / f_{22}^{\text{RD}}$ ,  $f_0^\varphi = 0.014 f_{\ell m}^{\text{RD}} / f_{22}^{\text{RD}}$ , and  $f_{\ell m}^{\text{RD}} = \omega_{\ell m 0} / 2\pi$ , where  $\omega_{\ell m 0}$  is the real-valued frequency of the fundamental QNM.

The frequency mapping above is sufficient to relate the frequency-domain phase derivatives of all multipoles to each other,  $\varphi'_{\ell m}(f) = \varphi'_{22}[f_{\ell m}(f)]$ . Integrating once yields the phase relation that contains the inverse of the derivative of  $f_{\ell m}$  (where we understand the derivative at each boundary as the limit from lower frequencies toward that boundary). The additional, multipole-dependent phase offsets are determined from PN theory and by imposing continuity. The resulting coefficients read

$$\begin{aligned} \kappa_{\ell m} &= \frac{1}{f'_{\ell m}(f)}, \quad (\text{piecewise constant}) \\ \Delta_{\ell m} &= \begin{cases} \frac{\pi}{2} [3\ell + \text{mod}(\ell + m, 2)] - \pi, & f \leq f_0^\varphi \\ \varphi_{\ell m}(f_0^\varphi) - \kappa_{\ell m} \varphi_{22}[f_{\ell m}^\varphi(f_0^\varphi)], & f_0^\varphi < f \leq f_{\ell m}^{\text{RD}} \\ \varphi_{\ell m}(f_{\ell m}^{\text{RD}}) - \varphi_{22}[f_{\ell m}^\varphi(f_{\ell m}^{\text{RD}})], & f > f_{\ell m}^{\text{RD}}. \end{cases} \end{aligned} \quad (6)$$

The phase shifts introduced explicitly for  $f < f_0^\varphi$  reflect mass and current multipole separation (see e.g., Equation 326 of [19]) as well as the necessary symmetry properties of each multipole [19, 20].

Equations (3-7) constitute a minimalistic model-agnostic method to map the dominant into subdominant multipoles.

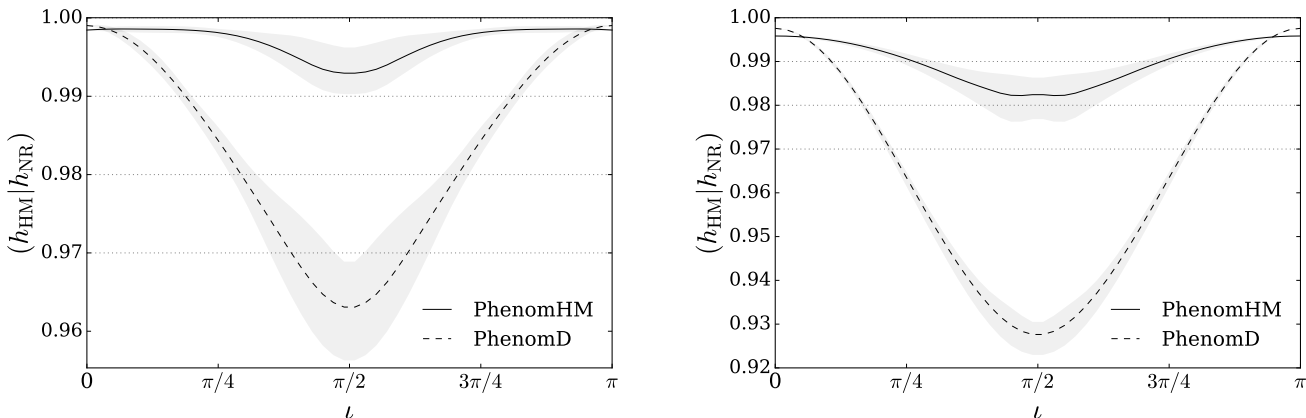


Figure 3. Matches (*faithfulness*) between PhenomHM and NR for (*Left*)  $m_1/m_2 = 2$ ,  $\chi_{1z} = \chi_{2z} = -0.5$  and (*Right*)  $m_1/m_2 = 4$ ,  $\chi_1 = \chi_2 = 0.5$  binary BH systems. Each case has a total mass of  $90 M_\odot$  with a minimum frequency of  $20 \text{ Hz}$ . In both cases, the black lines show volume weighted average matches, and the grey bands display the range of possible values with varying signal polarization and orbital phase. Here the NR waveform contains all multipoles up to  $\ell = 5$ , while PhenomHM contains multipoles with  $\ell = |m| \leq 4$  and  $|m| = \ell - 1$ .

*Application to PhenomD* – Upon choosing a model for the dominant multipole waveform, further refinements may be applied. Here we consider PhenomD [13, 17].

Comparison with NR data shows that the phase that results from Equation (5) is least accurate for frequencies just below  $f_{\ell m}^{\text{RD}}$ . For frequencies below  $f_{\ell m}^{\text{RD}}$ ,  $f_{\ell m}(f)$ 's linear interpolation does not ensure a simple shift from  $f_{22}^{\text{RD}}$  to  $f_{\ell m}^{\text{RD}}$ , but rather a shift with some non-unity slope. This could be improved by using a different frequency mapping in the intermediate region, but a linear mapping has the advantage that we can analytically integrate the phase derivative. Alternatively, we can modify the underlying PhenomD phase ansatz.

We find that a simple extension of the PhenomD phase ansatz as well as a compatible adjustment of  $f_{\ell m}(f)$  for  $f > f_{\ell m}^{\text{RD}}$  are sufficient to impart the correct behavior prior to the ringdown frequency. In the merger-ringdown phase ansatz, Eq. (14) of Ref. [13], we add factors of  $f_{22}^{\text{RD}}/f_{\ell m}^{\text{RD}}$  to the last term, and use the appropriate damping frequency for each mode. The modified parts of the model are,

$$f_{\ell m}(f) = \begin{cases} \frac{f_{22}^{\text{RD}}}{f_{\ell m}^{\text{RD}}} f, & f > f_{\ell m}^{\text{RD}} \\ \text{see (5)} & \text{otherwise,} \end{cases} \quad (8)$$

$$\phi_{\text{MR}}^{\ell m}(f) = \frac{1}{\eta} \left\{ \alpha_0 + \alpha_1 f - \alpha_2 f^{-1} + \frac{4}{3} \alpha_3 f^{3/4} + \alpha_4 \frac{f_{22}^{\text{RD}}}{f_{\ell m}^{\text{RD}}} \tan^{-1} \left( \frac{f - \alpha_5 f_{22}^{\text{RD}}}{\frac{f_{22}^{\text{RD}}}{f_{\ell m}^{\text{RD}}} f_{\ell m}^{\text{damp}}} \right) \right\}. \quad (9)$$

Equations (3-9) define a GW signal model extended to higher multipoles via the mapping of PhenomD. We refer to this extended multipole model as PhenomHM.

*Results* – We assess the accuracy and utility of PhenomHM through comparisons with NR simulations. We use NR simulations over the same parameter range that was used in the calibration of the dominant-multipole PhenomD model, which includes simulations performed with the BAM [21, 22] and SpEC [23] codes; the latter were taken from the public SXS waveform catalog [24]. These cover mass ratios from 1:1 to 1:18, and spin magnitudes up to 0.85 (and up to 0.98 for equal-mass configurations). The tests we perform of the PhenomHM

model are threefold. The first is a basic check that an inverse Fourier transform produces qualitatively correct time-domain waveforms without pathological features. Such features are sometimes only cosmetic, but their absence serves as an elementary assessment of the robustness of our method. Secondly, we calculate a noise-weighted inner product (match) between the NR waveforms and the model, for a range of binary inclinations, waveform polarisations, and choice of initial phase. This allows us to approximately estimate the accuracy of the model, which is crucial for gravitational-wave (GW) search and parameter-estimation purposes. Finally, we perform a suite of parameter-estimation calculations in order to gauge the impact of higher-multipoles on GW measurements. We discuss a representative sample of our match and parameter-estimation results below.

To quantify how PhenomHM compares to NR, we calculate the match weighted by the aLIGO noise power spectrum,  $S_n(f)$ ; we use the anticipated zero detuned, high power, design sensitivity [14]. A binary source configuration is defined by  $(M, \eta, \chi_1, \chi_2)$ , where  $\chi_1$  and  $\chi_2$  denote the projections of the dimensionless spins of the two BHs onto the direction of the orbital angular momentum. For a signal with some choice of inclination  $\iota$ , polarisation  $\psi_S$ , and initial orbital phase  $\phi_{0S}$ , the match against NR data is calculated for a PhenomHM template waveform with the same parameters  $(M, \eta, \chi_1, \chi_2, \iota)$ , but optimised over the time of arrival  $t_0$ , the template's polarization  $\psi_M$  and initial orbital phase  $\phi_{0M}$ . Specifically, we compute the inner product

$$(h_{\text{HM}}|h_{\text{NR}}) \equiv 4 \text{Re} \int_{f_{\text{min}}}^{f_{\text{max}}} \frac{\tilde{h}_{\text{HM}}(f) \tilde{h}_{\text{NR}}^*(f)}{S_n(f)} df \quad (10)$$

normalised by  $\sqrt{(h_{\text{HM}}|h_{\text{HM}})(h_{\text{NR}}|h_{\text{NR}})}$ , and then maximised with respect to  $(\psi_M, \phi_{0M}, t_0)$  [25, 26]. The NR waveforms contain all multipoles with  $\ell \leq 5$  and the PhenomHM waveforms include multipoles with  $\ell = |m| \leq 4$  and  $|m| = \ell - 1$ . We choose  $f_{\text{min}} = 20 \text{ Hz}$ .

Figure 3 presents the result for two example binary BH systems. As the matches vary with the source's polarisation and

orbital phase angles, we show average values after appropriately accounting for variations in the signal strength, i.e., we volume-weight them by the signal-to-noise ratio (SNR) cubed (see, e.g., Ref. [8]). For face-on ( $\iota = 0$ ) and face-off inclinations ( $\iota = \pi$ ), we observe the match to marginally decrease with respect to PhenomD due to inaccuracies in the PhenomHM ( $l, m$ ) = (3, 2) and (4, 4) multipoles. However, in both cases we see that PhenomHM displays consistently higher matches than PhenomD for inclined systems. As the mass ratio increases, the performance of the dominant-multipole PhenomD model rapidly degrades for edge-on configurations, but remains high for PhenomHM.

We find that for nonspinning systems, PhenomHM typically has matches higher than 0.99 for all mass ratios. The matches degrade for high-mass-ratio, high-aligned-spin systems with edge-on inclination, and the match average over polarisation and initial phase can be as low as 0.93, for a mass-ratio 1:8 system with  $\chi_1 = 0.85$ . However, the worst matches correspond to choices of both polarisation and inclination that suppress the dominant mode, making these signals significantly weaker, and therefore less likely to be observed.

We expect that the main value of PhenomHM will be in parameter recovery. To assess this, we performed an analysis similar to the one carried out in Ref. [27]: we injected NR waveforms into zero noise [28], and then estimated the parameters using the same Bayesian inference codes employed in GW observations [4, 29, 30], and compared results obtained using PhenomHM as recovery model against ones obtained using PhenomD. For configurations with a variety of mass ratios and spins, we found that the inaccuracies in PhenomHM did not lead to appreciable biases in recovering masses and spins for SNRs of  $\sim 25$ ; a more detailed parameter-estimation study is in preparation.

In comparisons between PhenomD and PhenomHM, the most striking result was that the higher-multipole PhenomHM model can lead to a significant improvement in measurements of the source inclination. This is not surprising: as we see in Fig. 2, different binary orientations are much more clearly distinguishable when higher multipoles are included in the signal. In Fig. 4 we show an example of a  $90 M_\odot$  binary with mass ratio 4 and spins  $\chi_1 = \chi_2 = 0.5$ , at a distance of 583 Mpc. Since face-on systems are the most likely to be detected (they are roughly twice as strong as edge-on systems, meaning that they can be observed in a volume of the universe eight times larger), we inject the signal face-on to the detector. Using PhenomD, we recover only our prior expectation of the inclination, and the 90% credible region for the distance runs from 300 Mpc to 746 Mpc. All GW observations to date display results similar to this [2–4]. When using PhenomHM, however, the opening angle of the binary is recovered with an uncertainty of only 0.24 radians (14 degrees), although there is some degeneracy between face-on and face-away signals. The uncertainty in distance is approximately reduced by 20%, with the 90% credible region ranging from 489 Mpc to 831 Mpc. The uncertainty in the distance is now due predominantly to the uncertainty in the sky localisation; sky localisation will typically be far better with a three-detector network [31]. Both models recover the injected distance.

*Discussion* – We have presented a simple and flexible method to transform the dominant GW multipole into higher multipoles for non-precessing binary BH systems. This may be applied to any dominant-multipole-only frequency-domain

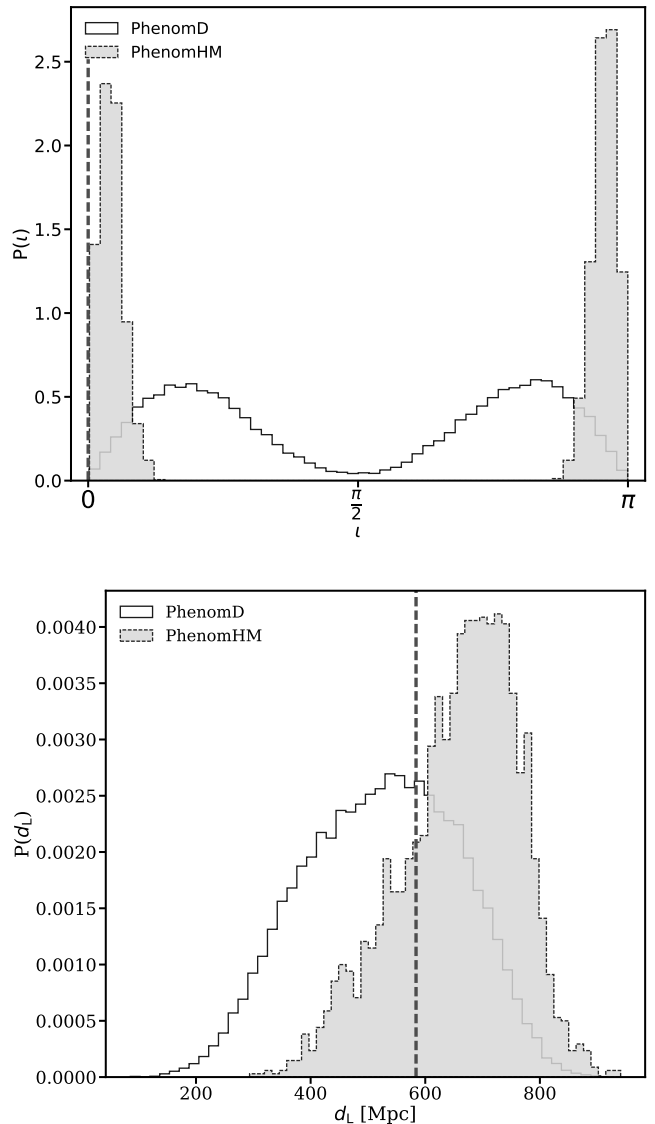


Figure 4. Parameter recovery for a  $90 M_\odot$  mass-ratio 4 binary, with aligned spins  $\chi_1 = \chi_2 = 0.5$ , optimally oriented to the detector at a distance of 583 Mpc. Use of the higher-multipole PhenomHM model allows us to correctly identify the source orientation, and the uncertainty in the distance is reduced by approximately 20%.

model. We also introduced the first application of this method, by taking the phenomenological model PhenomD [13, 17] and producing a more accurate higher-multipole model, which we call PhenomHM.

For inclined systems, we find that the PhenomHM model agrees better with NR waveforms than the dominant-multipole-only PhenomD model, across the entire calibration region of the underlying PhenomD, mass ratios up to 1:18, and spins up to 0.85. For high-mass-ratio systems, matches between NR data and PhenomD waveforms can be as low as 0.7, for particular edge-on orientations, while PhenomHM typically yields an average match above 0.95. In a first suite of parameter-estimation tests, we have found that even for face-on systems, where the higher-multipole contribution to the signal is weak, PhenomHM produces a dramatic improvement over PhenomD in recovering the source inclination and also improvement in distance.

It is striking that simple approximations can be used to model the subdominant multipoles. In particular, we stress that a single overall scaling factor is sufficient to capture the qualitative behaviour of the signal amplitude, throughout the inspiral, merger, and ringdown. This approach suggests that any frequency-domain model for the dominant multipole can be easily extended to higher multipoles (including models that treat precession), and suggests a means to rapidly improve current waveform models. An extension of PhenomHM to precession will be presented in the near future.

Despite its encouraging performance in the tests we have performed, further studies are needed to fully quantify the value of PhenomHM in GW astronomy. There are also many avenues for improvement. It may be possible to make better choices for the transition frequencies between the mapping regions, and to improve on the linear frequency interpolation between the inspiral and merger-ringdown regimes. Beyond that, the most obvious next step is to use PhenomHM as the basis for a precise tuning of the subdominant multipoles to NR waveforms. This work is underway. Several physical features are also absent from this model. The most notable of these is the mixing between the  $|m| = \ell$  and  $|m| = \ell - 1$  multipoles through merger and ringdown [32]. An obvious extension to precessing systems, following the prescription of PhenomP [33], would also neglect to model the multipole asymmetry between the  $m > 0$  and  $m < 0$  multipoles that leads to out-of-plane recoil [34].

However, given that the model captures the phenomenology of the subdominant multipoles across the binary BH parameter space, and shows mismatch errors of at most a few

percent, and for much of the parameter space less than 1%, PhenomHM will make it possible to assess the importance of subdominant multipoles in GW observations, and improve the accuracy and reduce the uncertainties in parameter estimates. For high-mass binaries, where the merger and ringdown dominate the signal, it will also be valuable in strengthening current tests of general relativity.

*Acknowledgements* – We thank Geraint Pratten and Cecilio García Quiros for useful discussions. We thank P. Ajith and Chandra Mishra for useful discussions and for sharing a draft on their recently completed nonspinning higher multipole model. We also thank R. Cotesta, A. Bohé, A. Buonanno and A. Taracchini for making us aware of their progress towards a higher multipole model in the EOBNR framework. The work presented in this paper was supported by Science and Technology Facilities Council (STFC) grant ST/L000962/1, European Research Council Consolidator Grant 647839, the Max Planck Society, Spanish Ministry of Economy and Competitiveness grants CSD2009-00064, FPA2013-41042-P and FPA2016-76821-P, the Spanish Agencia Estatal de Investigación, European Union FEDER funds, Vicepresidència i Conselleria d’Innovació, Recerca i Turisme, Conselleria d’Educació, i Universitats del Govern de les Illes Balears, and the Fons Social Europeu. BAM simulations were carried out at Advanced Research Computing (ARCCA) at Cardiff, as part of the European PRACE petascale computing initiative on the clusters Hermit, Curie and SuperMUC, on the UK DiRAC Datacentric cluster and on the BSC MareNostrum computer under PRACE and RES (Red Española de Supercomputación) allocations.

- 
- [1] B. P. Abbott *et al.*, “Observation of Gravitational Waves from a Binary Black Hole Merger,” *Phys. Rev. Lett.*, vol. 116, no. 6, p. 061102, 2016.
- [2] B. P. Abbott *et al.*, “GW151226: Observation of Gravitational Waves from a 22-Solar-Mass Binary Black Hole Coalescence,” *Phys. Rev. Lett.*, vol. 116, no. 24, p. 241103, 2016.
- [3] B. P. Abbott *et al.*, “GW170104: Observation of a 50-Solar-Mass Binary Black Hole Coalescence at Redshift 0.2,” *Phys. Rev. Lett.*, vol. 118, no. 22, p. 221101, 2017.
- [4] B. P. Abbott *et al.*, “Properties of the Binary Black Hole Merger GW150914,” *Phys. Rev. Lett.*, vol. 116, no. 24, p. 241102, 2016.
- [5] T. D. Abbott *et al.*, “Improved analysis of GW150914 using a fully spin-precessing waveform Model,” *Phys. Rev.*, vol. X6, no. 4, p. 041014, 2016.
- [6] B. P. Abbott *et al.*, “Binary Black Hole Mergers in the first Advanced LIGO Observing Run,” *Phys. Rev.*, vol. X6, no. 4, p. 041015, 2016.
- [7] C. Capano, Y. Pan, and A. Buonanno, “Impact of higher harmonics in searching for gravitational waves from nonspinning binary black holes,” *Phys. Rev.*, vol. D89, no. 10, p. 102003, 2014.
- [8] V. Varma and P. Ajith, “Effects of non-quadrupole modes in the detection and parameter estimation of black hole binaries with nonprecessing spins,” 2016.
- [9] J. Calderón Bustillo, P. Laguna, and D. Shoemaker, “Detectability of gravitational waves from binary black holes: Impact of precession and higher modes,” *Phys. Rev.*, vol. D95, no. 10, p. 104038, 2017.
- [10] J. Lange *et al.*, “A Parameter Estimation Method that Directly Compares Gravitational Wave Observations to Numerical Relativity,” 2017.
- [11] Y. Pan, A. Buonanno, M. Boyle, L. T. Buchman, L. E. Kidder, H. P. Pfeiffer, and M. A. Scheel, “Inspiral-merger-ringdown multipolar waveforms of nonspinning black-hole binaries using the effective-one-body formalism,” *Phys. Rev.*, vol. D84, p. 124052, 2011.
- [12] J. Blackman, S. E. Field, M. A. Scheel, C. R. Galley, C. D. Ott, M. Boyle, L. E. Kidder, H. P. Pfeiffer, and B. Szilágyi, “A Numerical Relativity Waveform Surrogate Model for Generically Precessing Binary Black Hole Mergers,” 2017.
- [13] S. Khan, S. Husa, M. Hannam, F. Ohme, M. Pürrer, X. Jiménez Forteza, and A. Bohé, “Frequency-domain gravitational waves from nonprecessing black-hole binaries. II. A phenomenological model for the advanced detector era,” *Phys. Rev.*, vol. D93, no. 4, p. 044007, 2016.
- [14] D. Shoemaker *et al.*, “Advanced ligo anticipated sensitivity curves,” *LIGO-T0900288*, <https://dcc.ligo.org/cgi-bin/DocDB/ShowDocument?docid=2974>, 2010.
- [15] S. Hild *et al.*, “Sensitivity Studies for Third-Generation Gravitational Wave Observatories,” *Class. Quant. Grav.*, vol. 28, p. 094013, 2011.
- [16] J. N. Goldberg, A. J. MacFarlane, E. T. Newman, F. Rohrlich, and E. C. G. Sudarshan, “Spin s spherical harmonics and edth,” *J. Math. Phys.*, vol. 8, p. 2155, 1967.
- [17] S. Husa, S. Khan, M. Hannam, M. Pürrer, F. Ohme, X. Jiménez Forteza, and A. Bohé, “Frequency-domain gravitational waves from nonprecessing black-hole binaries. I. New numerical waveforms and anatomy of the signal,” *Phys. Rev.*, vol. D93, no. 4, p. 044006, 2016.
- [18] T. Damour, B. R. Iyer, and B. S. Sathyaprakash, “Frequency domain P approximant filters for time truncated inspiral gravitational wave signals from compact binaries,” *Phys. Rev.*, vol. D62, p. 084036, 2000.

- [19] L. Blanchet, “Gravitational Radiation from Post-Newtonian Sources and Inspiralling Compact Binaries,” *Living Rev. Rel.*, vol. 17, p. 2, 2014.
- [20] L. E. Kidder, “Using full information when computing modes of post-Newtonian waveforms from inspiralling compact binaries in circular orbit,” *Phys. Rev.*, vol. D77, p. 044016, 2008.
- [21] B. Brügmann, J. A. González, M. Hannam, S. Husa, U. Sperhake, and W. Tichy, “Calibration of Moving Puncture Simulations,” *Phys. Rev.*, vol. D77, p. 024027, 2008.
- [22] S. Husa, J. A. González, M. Hannam, B. Brügmann, and U. Sperhake, “Reducing phase error in long numerical binary black hole evolutions with sixth order finite differencing,” *Class. Quant. Grav.*, vol. 25, p. 105006, 2008.
- [23] M. A. Scheel, H. P. Pfeiffer, L. Lindblom, L. E. Kidder, O. Rinne, and S. A. Teukolsky, “Solving Einstein’s equations with dual coordinate frames,” *Phys. Rev.*, vol. D74, p. 104006, 2006.
- [24] <http://www.black-holes.org/waveforms>.
- [25] P. Schmidt, F. Ohme, and M. Hannam, “Towards models of gravitational waveforms from generic binaries II: Modelling precession effects with a single effective precession parameter,” *Phys. Rev.*, vol. D91, no. 2, p. 024043, 2015.
- [26] I. Harry, S. Privitera, A. Bohé, and A. Buonanno, “Searching for Gravitational Waves from Compact Binaries with Precessing Spins,” *Phys. Rev.*, vol. D94, no. 2, p. 024012, 2016.
- [27] B. P. Abbott *et al.*, “Effects of waveform model systematics on the interpretation of GW150914,” *Class. Quant. Grav.*, vol. 34, no. 10, p. 104002, 2017.
- [28] P. Schmidt, I. W. Harry, and H. P. Pfeiffer, “Numerical Relativity Injection Infrastructure,” 2017.
- [29] J. Veitch *et al.*, “Parameter estimation for compact binaries with ground-based gravitational-wave observations using the LALInference software library,” *Phys. Rev.*, vol. D91, no. 4, p. 042003, 2015.
- [30] <https://wiki.ligo.org/DASWG/LALSuite>.
- [31] B. P. Abbott *et al.*, “Prospects for Observing and Localizing Gravitational-Wave Transients with Advanced LIGO and Advanced Virgo,” 2013. [Living Rev. Rel.19,1(2016)].
- [32] L. London, D. Shoemaker, and J. Healy, “Modeling ring-down: Beyond the fundamental quasinormal modes,” *Phys. Rev.*, vol. D90, no. 12, p. 124032, 2014. [Erratum: *Phys. Rev.*D94,no.6,069902(2016)].
- [33] M. Hannam, P. Schmidt, A. Bohé, L. Haegel, S. Husa, F. Ohme, G. Pratten, and M. Pürrer, “Simple Model of Complete Precessing Black-Hole-Binary Gravitational Waveforms,” *Phys. Rev. Lett.*, vol. 113, no. 15, p. 151101, 2014.
- [34] B. Brügmann, J. A. González, M. Hannam, S. Husa, and U. Sperhake, “Exploring black hole superkicks,” *Phys. Rev.*, vol. D77, p. 124047, 2008.